Fabrication and Characterization of Niobium Diffusion-Cooled Hot-Electron Bolometers on Silicon Nitride Membranes

Aaron M. Datesman, Jonathan C. Schultz, Arthur W. Lichtenberger, Dathon Golish, Christopher K. Walker, and Jacob Kooi

Abstract — **We have successfully fabricated niobium diffusion-cooled hot-electron bolometer (HEB) mixers on membranes of silicon nitride less than one micron thick. This advance has allowed us to construct a 1x5 HEB receiver array intended for operation at 1.45 THz. This article provides an overview of the integration of the HEB array chip with silicon micromachined backshorts and feedhorns, discusses materials issues surrounding the device fabrication, reports resistance and I-V measurements, and compares HEBs fabricated on silicon nitride to similar devices on quartz substrates**.

Index Terms — **HEB, Mixer, Focused-ion beam, Membrane.**

I. Overview of Design & Construction of the Receiver

This article discusses our progress to date building a 1x5 heterodyne receiver array for operation at 1450 GHz. The receiver consists of niobium diffusion-cooled hot-electron bolometer mixers, fabricated on membranes of silicon nitride 0.75 μm thick [1], integrated with backshorts and feedhorns made from silicon using bulk chemical etching and/or laser micromachining [2]. Because the mixer rests on an electrically transparent membrane, the backshort in this design sits underneath the mixer chip; the feedhorn axis, mixer, and backshort are all co-linear. This allows several identical circuits to be replicated linearly on a single chip, creating a 1x5 array [3]. The receiver consists of three pieces, which we refer to as the backshort block, the HEB block, and the feedhorn block.

The HEB block is fabricated from a silicon wafer 127 μm thick, covered on both sides by low-stress LPCVD silicon nitride. The mixer circuitry (probe, filters, ground plane, and CPW, see Figure 1) is patterned from films of niobium and gold (Nb[10nm]/Au[300nm]/Nb[30nm]) deposited under a single vacuum using a liftoff stencil. Next, using backside alignment and RIE, windows for the membrane etch are opened; the membranes are released using a meniscus etching technique [4] which protects the circuitry on the front of the wafer from the caustic etchant. Then the arrays are diced, cleaned, and coated with a thin layer of gold for imaging during HEB fabrication, described in the next section.

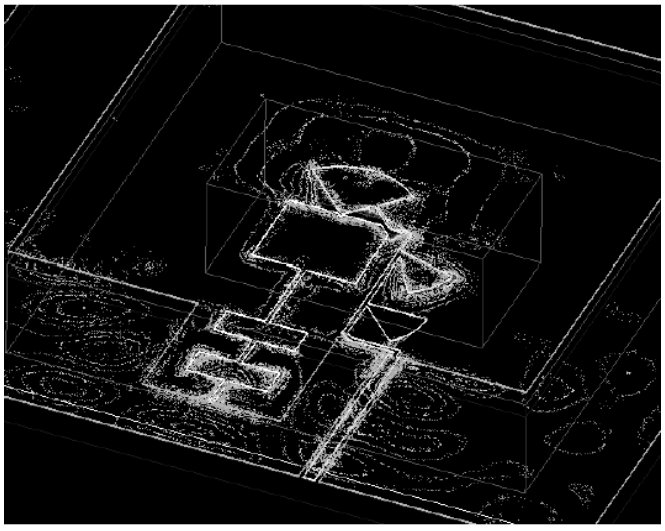

Fig. 1. Electric field shade plot detailing the operation of one pixel in the array of mixers. The HEB sits at the throat of the semicircular waveguide probe; the IF signal travels out through the 3 μm line tapping into the probe.

II. HEB Fabrication with a Focused-Ion Beam

A diffusion-cooled HEB consists of a short (less than 0.3 μm) bridge of superconducting thin film contacting pads of normal metal at each end, which act as heat sinks. Our efforts to fabricate these devices with a focused-ion beam (FIB) have evolved considerably since previous reports [5]; what follows is a summary of the current process.

A gallium focused-ion beam, interfaced with CAD control, can be used to mill away portions of a target substrate according to a user-defined pattern. Its use for the manufacture of arbitrary geometries has been reported in [6], and elsewhere. Our FIB fabrication technique involves three steps which sculpt an HEB from a patch of excess material at the probe throat, called the kernel. These steps are designated FIB1, FIB2, and FIB3, all occurring in a single session.

Manuscript received October 3, 2004. This work was supported under NSF grant #AST-0242525, NSF grant #AST-0138318 and NASA grant #NAG5-9100.

Aaron M. Datesman, Jonathan C. Schultz, and Arthur W. Lichtenberger (e-mail awl1l@virginia.edu) are with the University of Virginia Department of Electrical and Computer Engineering, Charlottesville, VA.

Dathon Golish and Christopher K. Walker are with the University of Arizona Steward Observatory, Tucson, AZ.

Jacob Kooi is with the California Institute of Technology, Pasadena, CA.

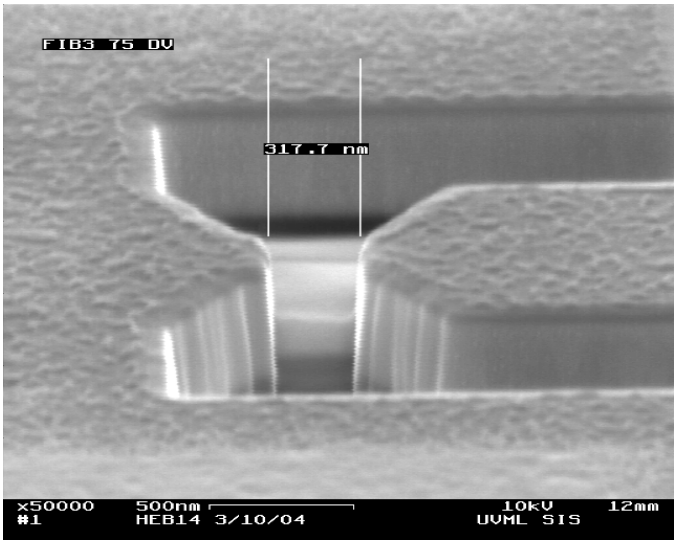

Fig. 2. The result of the FIB fabrication process, including a view of the CPW structure leading to the semicircular waveguide probe, which extends to the right out of the field of this picture. About 100 nm of gold remains atop this niobium microbridge after the FIB3 mill, which defines the length of this HEB as 318 nm. The FIB2 mill determines the width of the device.

FIB1 uses a high beam current (350 pA) to mill out from the 8 μm x 4 μm kernel a probe-to-CPW transition with features too fine to create reliably by lift-off. The microbridge is located at the terminus of this transition (see Figure 2). The FIB1 step kicks up a great deal of debris, which sticks to exposed gold surfaces. Performed at a low beam current (11 pA), FIB2 removes a small amount of material from the edges of the microbridge, cleaning off the shell of material left by FIB1. FIB3 is then performed with the same low beam current, but with the sample stage tilted at 45 degrees to the ion beam. This allows the user to remove the top layer of masking Nb and the top ~150 nm of Au without any possibility of harming the niobium microbridge underneath.

It is then necessary to remove the exposed gold remaining atop the HEB microbridge. We have attempted this using an iodine-based wet etchant with devices on a quartz substrate, often with good results (resistances uniform within 10%). However, undercutting of the 30 nm niobium mask at the ends of the bridge is a problem, and the etchant seems to damage the niobium film, causing devices to open-circuit over a time frame of a few weeks. Therefore it is necessary to remove the microbridge gold with a physical etch of 150 V argon ions in an RIE, which will be described shortly.

The fabrication of the 1x5 arrays is completed once the HEBs are passivated with a blanket layer of 100 nm of sputtered germanium. The Ge layer is patterned using a special resist and etched in the RIE in a chemistry which also removes the top level of niobium. It is found that devices passivated with germanium are much more robust than unpassivated devices. At temperatures above 130C, however, the sputtered germanium reacts with the niobium film it covers [7], degrading or destroying the devices, which are otherwise reasonably robust.

III. Stress of Sputtered Niobium Films

The films described in this work were deposited under a single vacuum in a multi-target sputtering system with a base pressure in the mid-10^{-8} torr range. To measure the stress of deposited niobium films, a strict protocol of preparing the sputtering guns and cleaning the substrate with an in-situ ion clean was followed. These results refer to the stress in a 2000 Å Nb film, deposited either on a 300 μm thick silicon wafer, covered with 1000 Å of silicon dioxide, or on silicon wafers of various thicknesses, covered with between 0.75 - 1 μm of LPCVD silicon nitride. The stress was typically measured using laser interferometry, allowing the film stress to be inferred from the measured curvature of the wafer.

Deposition on to Si/SiO_2 substrates was found to be highly repeatable and controllable, with a change in sputtering chamber pressure of 0.05 microns reliably corresponding to a change in the film stress of approximately 50 MPa. Profilometry stress measurements verified that niobium films on Si/SiO_2 exhibited the same stress as films sputtered on quartz wafers under the same conditions [8]. Niobium films sputtered on to Si/LPCVD nitride substrates under those conditions, however, are found to be extremely compressive (typically -300 to -500 MPa). The measured film stress was additionally not repeatable from wafer to wafer, and did not show any noticeable trend toward becoming zero-stress with increasing chamber pressure. This was true for tests involving silicon nitride films provided by two separate sources.

The niobium films sputtered on to silicon/LPCVD silicon nitride substrates described in this work were deposited at modestly higher pressure than that found to be optimal for Si/SiO_2 substrates, in an attempt to compensate for the highly compressive film stresses which were measured.

IV. Effects of Implanted Gallium on Superconducting Niobium Thin Films

Simulations with SRIM [9] give 95 Å as the range of 30 kV gallium ions in gold, with a 56 Å straggle. SRIM likewise verifies that there is essentially no likelihood of gallium ions backscattering from either quartz or silicon substrates up into the niobium layer, due to the relatively great weight of the ion. With this information, it is possible to identify the stages of the fabrication process which implant gallium into the niobium microbridge.

One concludes that the FIB2 step is likely to implant much more gallium into the microbridge than the FIB1 and FIB3 steps, but only into its edges. Since the microbridge is typically at least 1000 Å wide, it is reasonable to estimate that 80% or more of the width of the HEB should be free of contamination. Nevertheless, it is of interest to consider what the effects of this contamination might be. To this end, samples of Au[100 Å]/Nb[100 Å] on quartz substrates were prepared, irradiated with gallium using the FIB, and measured.

SRIM predicts that 35% of the ions incident upon this structure will stop within the niobium layer, although with a

very non-uniform dose profile. The average dose within the film is therefore estimated to be on the order of 10^{19} atoms/cm^3. The correlation between average dose and transition temperature for two sets of samples is shown in Figure 3. More information can be found in [10].

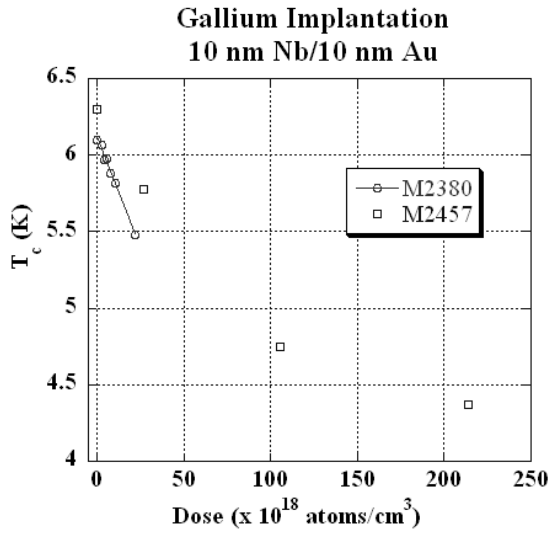

Fig. 3. Measurements of critical temperature vs. implanted gallium dose. The two sets of samples were deposited in our multi-target sputtering system many months apart; changes in the sputtering conditions or the thickness monitor settings probably explain the discrepancy between the two sets of data. Note that the sacrificial layer of 10 nm of Au is likely partially sputtered away during implantation; however, since a reduced gold thickness should reduce the proximity effect and thereby increase T_c, the effect of gallium implantation is accurately demonstrated here.

The FIB2 mill, which cleans the edges of the microbridge of material sputtered up by the FIB1 process, has the potential to implant a large dose of Ga into the edges of the microbridge. This step, however, sputters away the niobium film underneath the pattern it mills, as well as more than 3000 Å of overlying niobium and gold. Therefore, whatever gallium is implanted into the edges of the microbridge must travel there obliquely, cannot arrive by backscattering out of the substrate, and is certainly less than the 10^{20} cm^{-3} which has been shown here to merely suppress superconductivity in the Nb film.

V. Physical Removal of Gold with Argon RIE

To remove the 1000 - 2000 Å of gold remaining on top of the niobium microbridge after the FIB3 step, a physical etch using argon ions at a low voltage works reasonably well. At 300 Volts, an etch rate of approximately 100 Å/min results. Large-area niobium films respond robustly to this treatment; an etch of 12 minutes reduces the critical temperature from 6.35 K to 5.78 K, while increasing the resistance of the sample by 12 Ohms. However, the small feature size, sharp corners and high aspect ratio of the structure to be etched seem to concentrate the electric field within the RIE plasma, so that the HEBs do not respond robustly under identical conditions. (It should be noted that HEB fabrication techniques based upon e-beam lithography [11] also generally require sputter removal of gold with argon, but typically thicknesses of only 10-30 nm are involved.)

Reducing the self-bias to 150 Volts produces reasonable results after long etch times (2 hours is typical). The measured etch rate on large, smooth areas with these etch conditions is around 3 Å/min. if the sample is not heat-sunk to its glass carrier, and 9 Å/min. if it is lightly greased. Since even the higher rate does not suffice to explain the faster etching on actual HEB devices which verifiably occurs, geometrical enhancement of the etch rate seems reasonably certain, even if the exact mechanism is not totally clear.

In addition to being difficult to characterize, the bridge etch which completes the HEBs is not anisotropic and not as uniform as anticipated. Under ion bombardment, as a material gold tends to form "blobs" which decrease in volume as etching continues by retreating from their outside edges; that is, the film piles up upon itself. This explains the behavior of a series of microbridges of increasing length (0.2, 0.3, up to 0.6 microns) which were fabricated and etched, all of which turned out to be between 80-100 nm shorter than the corresponding gap in the niobium mask above. This occurs because, instead of the situation where the last tiny thickness of gold is cleared from the entire microbridge surface all at once - or over a short time - the center of the bridge is the first part to be exposed, after which the exposed area slowly increases as the overlying gold film creeps toward the protected gold surfaces at each end of the bridge. This effect is very significant due to the substantial thickness of gold which must be removed.

The inability to remove gold in an epitaxial fashion, along with the probability that the machine-aligned FIB3 process leaves behind different thicknesses of gold from one device to the next, most likely explains why the HEBs seem to etch at different rates. For example, a set of 4 samples on a quartz substrate after two hours of etching at 150 Volts had resistances of 6, 32, 19, and 24 Ω (at room temperature). An additional 75 minutes of etching brought these resistances up to acceptable values, although with a significant variation - 95, 108, 87 and 121 Ω. On other occasions, perhaps owing to the conditioning or cleanliness of the RIE system, a continuous 90 minutes of etching sufficed.

On the simple criterion of having a sample device which can be tested and which superconducts, the yield of this process is quite good (typically 75% or better). While the devices are very sensitive to ESD, the large chip size (for the array) and the procedure by which the samples are greased down to a glass slide as a carrier, and handled only on the carrier, seem to be workable adaptations to this issue.

VI. Results and Conclusion

Several 1x5 arrays have been fabricated, and now await RF testing. Because the CPW lines are too small to probe, all of the measurements on Si/Si_3N_4 substrates presented herein apply to samples fabricated at the same time, and processed along with, the arrays.

Figure 4 shows, for comparison, resistive transitions of an unpassivated device on a quartz substrate and of a passivated device on a silicon nitride membrane. The first device, exposed to air for twelve hours before this curve was measured, underwent 3 hours and 15 minutes of bridge etching in total. The device on a membrane was etched for 3 hours and 40 minutes in total.

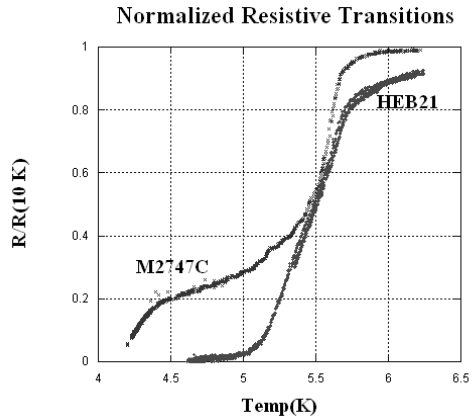

Fig. 4. Resistive transitions of two devices fabricated recently, normalized to their 10 Kelvins resistances. M2747C is an unpassivated device on a quartz substrate, R(10 K) = 76 Ω. HEB21 is a passivated device on a Si_3N_4 membrane, with R(10 K) = 43 Ω. 50 Ω is the resistance target.

The resistance ratios of these two devices, RRR = R(300 K)/R(10 K), were 1.6 and 1.4, respectively. The values of RRR, for devices on silicon nitride at least, vary a good deal even within the same batch of devices. Undamaged Nb films on quartz generally have resistance ratios around 2, sometimes as high as 2.3. Finally, niobium films on quartz in this work have generally had higher transition temperatures than films on silicon nitride, although T_c does tend to decrease as the film oxidizes. Oxidation is a very likely explanation for the lower-than-expected transition temperature of the unpassivated film, as well as for the different shapes of the curves presented in Figure 4.

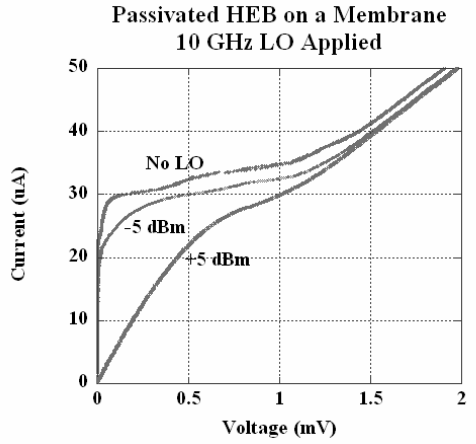

Fig. 5. I-V curves at 4.2 K for HEB21. The LO power is supplied through a coaxial cable, which is capacitively coupled to the pogo pins contacting the sample in the dipstick. The stated powers are merely relative measures of the power applied, and do not represent the power absorbed by the device.

Figure 5 shows the I-V curves for HEB21, including curves measured with 10 GHz power applied through a capacitively-coupled antenna. The critical current of the device, at 4.2 Kelvins, is a little more than 20 μA. Using material deposited in the same sputtering system and a newer fabrication process, one of us [12] has demonstrated I_c for a 150 Å niobium HEB on quartz in excess of 100 μA. All of the work described in this article involves 100 Å films, however, so a direct comparison is not available.

In conclusion, we have successfully fabricated the HEB block portion of a 1x5 receiver array for operation at 1.45 THz, and made substantial progress in the fabrication of the corresponding micromachined backshort and feedhorn blocks, and other associated hardware. Materials issues involving film stress, gallium contamination, and the physical etching of gold as a key step in the fabrication process were addressed. In general, the FIB fabrication process does not provide good control of the HEB device resistances, for which the difficult material properties of gold, and the amount of it which must be removed, are largely to blame. Germanium films were incorporated into the process successfully as a passivation material. Electrical measurements of the FIB-manufactured HEBs indicate that working devices which respond appropriately to RF radiation were fabricated. Future work will involve RF testing of these elements at 1.45 THz.

VII. Acknowledgements

Datesman would like to thank Jian Zhang, Alex Lobo, and Joe Beatrice for their contributions to this work.

References

[1] Provided by the Stanford Nanofabrication Facility, Palo Alto, CA.
[2] Walker, Drouet D'Aubigny, Groppi, Papapolymerou, Chin, and Lichtenberger, "A New Laser Micromachining System for the Fabrication of THz Waveguide and Quasi-Optical Components", 11th Int. Symp. on Space THz Tech., Ann Arbor, MI, May 2000.
[3] Walker, Groppi, Drouet D'Aubigny, Kulesa, Hedden, Prober, Siddiqi, Kooi, Chen, and Lichtenberger, "Integrated Heterodyne Array Receivers for Submillimeter Astronomy", SPIE Astronomical Telescopes and Instrumentation, 2002.
[4] Schultz, Ivanov, and Farmer, "Meniscus Interface Etching of Silicon in KOH in a Hands-on Introductory Course in MEMS", Proceedings of the 14th Biennial UGIM Symposium, pp. 153-157, VCU, Richmond, VA, 2001.
[5] Datesman, Zhang, and Lichtenberger, "A New Fabrication Technique for Ultra-Small Diffusion-Cooled Hot-Electron Bolometers", IEEE Transactions on Applied Superconductivity, Palm Desert, CA, 1998.
[6] Vasile, Niu, Nassar, Zhang, and Liu, "Focused ion beam milling: Depth control for three-dimensional microfabrication", J. Vac. Sci. Technol. B, Vol. 15, No. 6, pp. 2350-2354, 1997.
[7] Satow, "Structure Change of Amorphous Germanium in the Annealing Process", phys. stat. sol. (a), Vol. 18, pp. K147-K150, 1973.
[8] Thomas Cecil, University of Virginia, private communication.
[9] "The Stopping and Range of Ions in Matter", www.srim.org.
[10] Datesman, Cecil, Lyons, Schultz, and Lichtenberger, "Gallium Ion Implantation into Niobium Thin Films Using a Focused-Ion Beam", this proceedings.
[11] Robert B. Bass, Ph.D. Dissertation, Univ. of Virginia, 2004.
[12] Jon Schultz, University of Virginia, private communication.